JOURNAL OF GEOPHYSICAL RESEARCH, VOL. ???, XXXX, DOI:10.1029/,

Assessment of inter-calibration methods for satellite microwave humidity sounders

Viju O. John[1], Richard P. Allan[2], William Bell[3], Stefan A. Buehler[4], Ajil Kottayil[4]

Viju Oommen John, Met Office Hadley Centre, Exeter, UK, (viju.john@metoffice.gov.uk)

[1]Met Office Hadley Centre, Exeter, UK

[2]Department of Meteorology, University of Reading, UK

[3]Met Office, Exeter, UK

[4]Luleå University of Technology, Kiruna, Sweden

Abstract. Three methods for inter-calibrating humidity sounding channels are compared to assess their merits and demerits. The methods use: 1) Natural targets or vicarious calibration (Antarctica and tropical oceans), 2) zonal average brightness temperatures, and 3) simultaneous nadir overpasses (SNOs). Advanced Microwave Sounding Unit-B (AMSU-B) instruments onboard the polar-orbiting NOAA-15 and NOAA-16 satellites are used as examples. Antarctica is shown to be useful for identifying some of the instrument problems, but less promising for inter-calibrating humidity sounders due to the large diurnal variations there. Owing to smaller diurnal cycles over tropical oceans, these are found to be a good target for estimating inter-satellite biases. Estimated biases are more resistant to diurnal differences when data from ascending and descending passes are combined. Biases estimated from zonal averaged brightness temperatures show large seasonal and latitude dependence which could have resulted from diurnal cycle aliasing and scene-radiance dependence of the biases. This method may not be the best for channels with significant surface contributions. We have also tested the impact of clouds on the estimated biases and found that it is not significant, at least for tropical ocean estimates. Biases estimated from SNOs are free of diurnal cycle aliasing and cloud impacts.

1. Introduction

Water vapor in the troposphere (especially in the mid to upper troposphere) is an important climate variable due to its positive feedback in a warming climate [e.g., *Manabe and Wetherald*, 1967; *Held and Soden*, 2000]. Despite this, tropospheric water vapour is poorly simulated by current climate models [e.g., *John and Soden*, 2007]. Traditional water vapour measurements from radiosondes fail to provide an accurate and global picture of the distribution and evolution of water vapour in the mid to upper troposphere due to their inabilities to measure accurately in drier and colder conditions [e.g., *Soden and Lanzante*, 1996; *John and Buehler*, 2005]. Better sources of water vapour measurements with global coverage are satellite infrared (IR) and microwave (MW) measurements. The IR measurements have been used to understand the role of water vapour in the climate system [e.g., *Soden et al.*, 2005; *Shi and Bates*, 2011]. But there is a clear advantage in the microwave climate data record (CDR), which is the availability of all-sky data, whereas infrared records sample only clear areas [*John et al.*, 2011].

Satellite microwave humidity sounders have been measuring tropospheric water vapour for about 20 years with the first Special Sensor Microwave Humidity Sounder (SSM-T/2; [*Wilheit and al Khalaf*, 1994]) in orbit in November 1991. Later on, the first Advanced Microwave Sounding Unit-B (AMSU-B; *Saunders et al.* [1995]) was launched in May 1998, and the first Microwave Humidity Sounder (MHS; *Bonsignori* [2007]) was launched in May 2005. Microwave sounding data have been found to make significant impacts on the skills of Numerical Weather Prediction (NWP) [e.g., *Andersson et al.*, 2007]. However, SSM-T/2 data were not assimilated at NWP centres and the error characteristics of these measurements are poorly understood.

There have been efforts to inter-calibrate microwave humidity sounders [e.g., *John et al.*, 2012b] in order to provide climate quality data sets for climate monitoring and use in climate quality reanalyses. Inter-calibration methods which use simultaneous nadir overpasses (SNOs; [*Cao et al.*, 2004]) of polar orbiting satellites have become very popular [*Cao et al.*, 2005; *Shi et al.*, 2008; *Iacovazzi and Cao*, 2008; *Zou et al.*, 2009]. During an SNO, instruments on two satellites measure the same target area with short time differences, thus the difference in their measurements can practically be taken as inter-satellite bias. SNO estimates are free from some sampling errors, for example, arising from the diurnal cycle. However, SNOs of polar orbiting satellites normally occur only in polar latitudes (above 70°) and thus SNO measurements represent only a small portion of the dynamic ranges of global measurements [*Shi and Bates*, 2011]. It is shown in *John et al.* [2012b] that the scene-radiance dependence of inter-satellite biases limits the usefulness of polar-only SNOs for inter-calibrating microwave humidity sounders.

Another possible method for inter-calibration is the use of natural calibration targets such as Antarctica or tropical oceans [*Mo*, 2011]. *Mo* [2010] has shown that Antarctica can act as a good inter-calibration target during Antarctic winter months because diurnal variations there are very small. *Mo and Liu* [2008] have shown that tropical oceans can also act as a stable inter-calibration point. Therefore, in this study we analyse microwave humidity sounding data over these two natural targets to understand data characteristics and to estimate inter-satellite biases. The establishment of a set of natural Earth targets for instrument calibration is important for the calibration and validation of microwave radiometers [*Mo*, 2011].

Shi and Bates [2011] proposed and used another method for inter-calibrating upper tropospheric water vapour infrared radiances measured by different HIRS instruments. They used zonally averaged (10° bins) monthly mean brightness temperatures to estimate inter-satellite biases. They calculated radiance dependent biases for each satellite pair using zonally matched brightness temperatures. This method can be prone to errors from diurnal cycle variations [*Zou and Wang*, 2011].

We compare these three methods of inter-calibration - natural targets, SNOs, and zonal averages - for microwave humidity sounders by taking the AMSU-B instruments on NOAA-15 (N15) and NOAA-16 (N16) as examples. This study deals only with near-nadir brightness temperatures, thus avoiding any errors that could stem from scan-dependent biases. It is known that some of the AMSU-B channels have suffered from scan-dependent biases [*Buehler et al.*, 2005]. Also, this study discusses the methods which use only the data that has to be inter-calibrated (and not any other data or model outputs); thus minimising errors from other sources.

Another possible method for inter-calibration is the use of Observation minus Background (O–B) statistics from NWP analysis which is discussed in detail in *Saunders et al.* [2012] and therefore is not included in this study. One of the issues with (O–B) method is that known frequency changes are already modeled in the radiative transfer model used for assimilating observations and thus the impact of this on inter-satellite bias is not seen with this method. For example, radiance differences, as discussed in *John et al.* [2012b], due to change in central frequency from 150 to 157 GHz for Channel 2 of AMSU-B and MHS cannot be easily detected.

2. Data and methods

2.1. AMSU-B data

The AMSU-B is a 5 channel microwave radiometer which is designed to measure the radiation emitted from the Earth's surface and atmosphere in order to estimate global fields of tropospheric humidity. The instrument specifications are given in Table 1. AMSU-B is on-board NOAA-15 (N15), N16, and N17.

Channels 1 and 2 at 89 GHz and 150 GHz, respectively, enable deep penetration through the atmosphere to the Earth's surface. Channels 3–5 are located in the strongly opaque water vapor absorption line at 183.31 GHz and provide information on the tropospheric humidity at different levels. The passbands of Channels 3, 4, and 5 are at 183.31±1.00 GHz, 183.31±3.00 GHz, and 183.31±7.00 GHz, respectively.

At each channel frequency, the antenna beam-width (full width at half maximum) is a constant 1.1 degrees. Ninety contiguous cells are sampled on the Earth's surface, with each scan covering an angle of ±49.5 degrees from nadir. These scan patterns and geometric resolution translate to a 16.3 km diameter cell at nadir at a nominal satellite altitude of ∼833 km.

We obtained level 1b data of AMSU-B from the NOAA/CLASS digital library. Level 1b files contain quality controlled raw instrument counts. Geographical and operational calibration information is also included in the files. We used the ATOVS and AVHRR Processing Package (AAPP) to convert level 1b data to level 1c data. During this process the calibration coefficients are applied to the instrument counts to obtain antenna temperature and this is then converted to brightness temperatures by applying an antenna pattern correction [*Hewison and Saunders*, 1996]. Corrections for Radio Frequency Interference (RFI, [*Atkinson*, 2001]) are also done during the conversion to level 1c. We are already aware of quality issues of N15 and N16 AMSU-B data during their life times, but we include all the data here to see how bias estimates differ from method to method. Note that Channels 3, 4, and 5 of N15 failed in August 2010.

2.2. SNOs

SNOs were identified by the method developed by *Cao et al.* [2004]. SNOs occur with a frequency of about 8 days between N15 and N16. We used only 3 footprints on either side of nadir for analysis. We selected only those pixel pairs whose centres are less than 5 km apart and whose time difference is less than 300 seconds to avoid scene inhomogeneities affecting the estimated bias. These thresholds were estimated based on sensitivity analyses by *John et al.* [2012b]. We computed monthly bias and its standard error for the Northern and the Southern hemispheres separately. The results are shown on the left panels of Figure 6, but will be discussed later.

2.3. Zonal averages

The daily averages of the brightness temperatures were calculated by binning the data by latitude (1 ° grid) and then averaging them with weights proportional to the cosine of the latitudes for area weighting. We analyse ascending and descending passes separately in order to see the influence of the diurnal cycle. The results are shown in Figure 5, but will be discussed later.

2.4. Natural targets

We used the 1 ° zonal averaged daily near-nadir brightness temperatures to compute Antarctic mean values. We used Antarctic area weighted values from 70°S to 82°S.

To compute tropical ocean averages, we first gridded daily brightness temperatures to a 2.5°x2.5° latitude-longitude grid and then computed the area weighted average of ocean-only grid boxes from 20°S to 20°N.

3. Results

Figure 1 shows local equator crossing times (LECT) of ascending and descending nodes for N15 and N16. It can be clearly seen that orbital drift is significant for N15 and N16. When launched, N15, had equator crossing times at ∼7:30 AM/PM and by the end of 2010 that had become ∼4:30 AM/PM. N16 at launch had crossed the equator at ∼2 AM/PM and by the end of 2010 that had become ∼7 AM/PM. These changes in measurement time will have caused diurnal cycle aliasing which introduces non-climatic trends in the data records from these satellites which have to be taken into account before estimating inter-satellite biases.

Lindfors et al. [2011] have constructed diurnal cycles of infrared radiances, and the diurnal cycle of their surface channels will be comparable to those of Channel 1 and 2 of the microwave humidity sounders, at least qualitatively. Measurements over ocean showed an amplitude less than 1 K, but over the land it is of the order of 10 K. Their results show that the maximum of the diurnal cycle is at around 2 PM and the minimum at 4 AM.

Chung et al. [2007] describe the diurnal cycles of upper and mid tropospheric humidity. Similar to surface channels the amplitude is larger over land. For these channels the maximum occurs around 3 AM and the minimum at 4 PM over the land and 1PM over the ocean. Note that for any of these channels the cycles are not symmetric and therefore averaging ascending and descending passes, which are 12 hours apart, will not completely remove the diurnal cycle effects.

We also estimated climatological diurnal cycles for these channels using a method similar to *Lindfors et al.* [2011]. The work will be discussed in detail in *Kottayil et al.* [2012]. Our preliminary results concur with those of *Lindfors et al.* [2011] and *Chung et al.* [2007].

The following subsections discuss in detail the strengths and weaknesses of each of the three methods of inter-calibration.

3.1. Natural targets

3.1.1. Antarctica

Figure 2 shows time series of monthly mean near-nadir brightness temperatures observed over Antarctica (70°S–82°S) by the AMSU-B instruments on N15 (middle panels) and N16 (left panels) from 2001 to 2010. This analysis is similar to what is shown in *Mo* [2010] who studied AMSU-A brightness temperatures over Antarctica. Data for ascending (black curves) and descending (red curves) passes are separately processed as done in *Mo* [2010]. All channels show a distinct seasonal cycle with maxima occurring in Austral summer months and minima occurring in Austral winter months. Note that all channels do behave similarly, because over the elevated Antarctica all of them are surface channels, due to the very low water vapour column in the atmosphere [e.g., *John et al.*, 2012b]. The brightness temperatures decrease sharply to the minima at the start of autumn and stay low during the winter. The brightness temperatures then sharply increase to the maximum in late spring which basically depicts the seasonal cycle of Antarctic temperature. It is possible that there are secondary effects from changing emissivity due to changing surface type from pure ice or snow in winter to a mixture of water and snow in other seasons. Pure snow is known to have higher emissivity compared to a mixture of water and snow [*Mo*, 2011].

Blue curves in Figure 2 show the difference between ascending and descending passes. The axes labels are provided at the right hand side of each subplot. These differences are due to diurnal variations in the brightness temperatures. The differences show a clear seasonal cycle for all channels; small for Austral winter months and large for Austral summer months which is as expected. The differences are large for window/surface channels: up to 5 K for N16. But they are only about 1 K for Channel 3 which in Austral summer has only a partial contribution from the surface; the rest of the signal originates from the atmosphere where the diurnal cycle is weaker compared to the surface. The differences are larger for Channels 4 and 5 because they receive greater contributions from the surface.

The magnitude of the diurnal cycle differences for N16 is more than for N15 during early years because N15 was measuring in the early morning and evening whereas N16 was measuring in the afternoon and near midnight. Later on, due to orbit drift, these sampling times changed as shown in Figure 1 and the diurnal cycle differences decreased for N16 and increased for N15.

Mo [2010] showed that for AMSU-A channels the diurnal cycle differences become close to zero over Antarctica during Austral winter months which would be an ideal case for inter-calibration. This is almost the case for N16 AMSU-B channels, but not for N15 where ascending passes are warmer than descending passes during most years. Channel 4 of N15 shows the largest difference which began to increase around 2008 and in Austral winter of 2010 it reached 5 K. Also, the seasonal cycle for this channel is not clearly seen.

This channel is known to have problems due to RFI as discussed in Section 2.1. This clearly illustrates the usefulness of natural targets to identify periods of data problems and will be particularly useful for analysing data from the SSM-T/2 instrument whose data characteristics are poorly known.

Inter-satellite biases are shown in the right panels, separately for ascending (black curves) and descending (red curves) passes and also by combining both passes (green curves). Biases for ascending passes show a larger seasonal cycle. This is again because ascending passes are in the afternoon and evening and capture the seasonal modulation of the diurnal cycle, but descending passes are near midnight and early in the morning where diurnal cycle differences are smaller. This seasonal cycle of bias is stronger for surface channels and much weaker for sounding channels. One can expect that by combining ascending and descending passes, the diurnal cycle impact on estimated bias would be reduced. However, this does not completely eliminate the diurnal cycle effects because it only removes the 24 hour cycle component of the diurnal cycle and the diurnal cycles of microwave humidity sounder measurements are not just 24 hour cycles [*Kottayil et al.*, 2012].

It may be true that at the south pole there is no diurnal cycle during Austral winter months, but that may not be true for the Antarctic plateau as a whole [*Hudson and Brandt*, 2005]. Therefore, it is difficult to estimate inter-satellite biases using Antarctic measurements due to the impact of the diurnal cycle. This is especially true when biases are small. However, when the biases are larger, as is true for the sounding channels (3–5), these measurements can provide a qualitative idea of the inter-satellite biases, and show for example the sounding channels biases increase with time after 2007. Also, due to radiance dependence of the biases [e.g., *John et al.*, 2012b], estimated biases using Antarctic measurements may only be representative for the colder end of the brightness temperatures.

3.1.2. Tropical oceans

Tropical oceans are another suitable inter-calibration target where the microwave humidity sounding channels act differently from the Antarctic region. We gridded the near-nadir brightness temperatures over the tropical oceans (20°S–20°N) to construct daily averages. Channel 1 is always a window channel and thus sensitive to surface properties. Channel 2 acts mostly as a humidity sounding channel in the tropics, sensitive to the lowermost troposphere or boundary layer with very little contribution from the surface. However, it can have significant surface contributions in the dry subsidence zones of the tropics. Over tropical oceans, Channels 3-5 are humidity sounding channels with no contribution from the surface.

Figure 3 shows area weighted, tropical ocean averaged, near-nadir brightness temperatures for N15 and N16 AMSU-B channels. Contrary to measurements over Antarctica, the seasonal cycle is less pronounced. Also, the differences between ascending and descending passes show neither large differences nor seasonal dependence. This is because the range of diurnal variations in sea surface temperature is less than a Kelvin for tropical oceans [e.g., *Bernie et al.*, 2007; *Kennedy et al.*, 2007]. For both satellites Channels 1 and 2 do not show a large trend in brightness temperature time series, but significant trends can be seen for Channels 3, 4, and 5 of N16 and Channels 4 and 5 of N15 which probably is an indication of performance degradation of these channels.

It is interesting to note that the ascending passes (afternoon/evening) are colder than Descending passes for Channel 1, but the opposite is true for all other channels. The differences for Channel 1 increase with time for N15 and decrease with time for N16. In order to understand this different behaviour of Channel 1 we have estimated the diurnal cycle of Channel 1 brightness temperatures over tropical ocean which is shown in Figure 4. The Channel has highest values of brightness temperatures around midnight and the lowest during day time. For Channel 1, liquid water in clouds acts similarly to water vapour in the atmosphere and thus the reason for the late night or early morning peak in brightness temperatures over tropical ocean is likely to be due to signals from low level clouds. Diurnal cycle of marine stratocumulus clouds are also noticeable in infrared measurements (although here, minimum OLR is around 6 AM, the time of maximum cloud extent, since clouds reduce the upward emissions of infra-red radiation, see for example, Fig. 16d in *Allan et al.* [2007].

Channel 1 brightness temperature are warmer when the atmosphere has high liquid water content because more emission from the clouds will be added to the emission from the radiometrically colder ocean surface [*Sreerekha et al.*, 2008]. The liquid water content of low level clouds has maximum values in late night or early morning [*Wood et al.*, 2002]. Channel 1 shows opposite trends in biases for ascending and descending passes which is also related to sampling through different parts of the diurnal cycle which is shown in Figure 4. The biases become similar when the equator crossing times of the satellites are at the same time in 2008. This is an indication of strong diurnal cycles of liquid clouds over tropical oceans even though there is very little diurnal cycle for sea surface temperature.

Inter-satellite biases for N16–N15 are shown in the right panels of Figure 3, separately for ascending (black curves) and descending (red curves) passes. Unlike the biases estimated from Antarctic measurements, tropical ocean measurements show inter-satellite biases even for Channels 1 and 2, which was not apparent in the Antarctic measurements.

It is interesting to note that the seasonal variations of Channels 1 and 2 are similar for both satellites which indicates that these channels are in good order and have small biases in their measurements. Biases estimated for Channel 1 are mainly due to diurnal cycle effects, and combining ascending and descending passes has resulted in smaller biases. However, Channel 2 shows an increase in bias from close to zero in the early years to 1 K by the end of 2010.

Channel 3 shows an increasing inter-satellite bias starting in 2006. Looking at the brightness temperature time series plots for individual satellites, N16 is found to be responsible for a considerable part of this bias. There are distinct seasonal patterns in bias during this time period which resemble the solar beta angle of the satellite and are thus related to sun heating induced instrument temperature variability as shown in Figures 2 and 4 of *Zou and Wang* [2011]. Solar beta angle is defined as the angle between the orbit plane of the satellite and the vector from the Sun. The solar beta angle determines the amount of time the satellite spends in direct sunlight, absorbing solar energy.

Channel 4 brightness temperatures of N15 have an increasing trend for both passes during early years but then they remain flat for ascending passes and a deceasing trend for descending passes. The time series show abnormal, solar-angle related, seasonal variability which is more for the descending pass. N16 brightness temperatures shows an increasing trend for this channel. As a result of all these variabilities and trends this channel has large time-varying inter-satellite biases.

Channel 5 on N16 shows an anomalous decreasing trend for both ascending and descending nodes and on the other hand N15 brightness temperatures are showing a small increasing trend. As a result, this channel shows the largest bias which reaches 10 K by the end of 2010.

Over all, the analysis using tropical ocean averaged brightness temperatures shows more coherent patterns and time evolution of biases compared to the other natural target - Antarctica. This is mainly due to the comparatively smaller diurnal cycle for these measurements over tropical oceans. These results can be slightly affected by these smaller diurnal cycles, but combining measurements of the ascending and descending passes, which mitigates the diurnal cycle impact, can reduce the influence of diurnal cycle differences on the biases as shown by the green curves in Figure 3.

3.2. Zonal averages

In this section we analyse zonal averaged brightness temperatures of 10° wide latitude bands, which is similar to what was done in *Shi and Bates* [2011]. In fact, the two previous cases (Antarctica and tropical oceans) are special cases of the zonal average method. Figure 5 shows biases estimated using zonal mean brightness temperatures for the five channels using ascending (middle column), descending (right column) and both passes combined (left column) for N16–N15.

It was shown in *John et al.* [2012b] that biases estimated using zonal averaged brightness temperatures agrees well with the biases estimated using global SNOs for the sounding channels (Channels 3–5). However, it should be noted that global SNOs occur only when two satellites have similar equator crossing time (i.e., similar sampling times) and thus there is almost no influence of diurnal cycle differences in the zonal averaged brightness temperatures during those time periods. However, during other time periods diurnal cycle differences and orbit drift of the satellites can affect the estimated biases using this method.

Biases for Channel 1 and 2 (first and seconds rows, respectively, of Figure 5) show significant seasonal dependence outside the tropics even when both passes are used in bias estimation (when only ascending or descending passes are used latitudinal and seasonal dependences are even larger). Also, there is considerable latitude dependence for these biases. However, *John et al.* [2012b] have demonstrated using global SNOs that there is only very little latitude and scene-radiance dependence for the biases of these channels. Therefore, these significant latitudinal and seasonal variations of biases are likely to be a result of diurnal cycle effects mainly from the surface. This can be corroborated by the near-absence of latitude dependence in bias during mid-2008 when the sampling times of both satellites are similar.

Channel 3 (third row in Figure 5), on the other hand, shows very little latitude or seasonal dependence which is due to less surface influence and thus smaller diurnal cycle effects. Channel 4 (fourth row in Figure 5) biases show significant seasonal variability which is mainly due to the instrument being directly affected by sun angle variations as described in *Zou and Wang* [2011] and in the previous section. Some of this variability might also be coming from the diurnal cycle especially in recent years when the ascending and descending biases differ. Channel 5 (last row) bias shows latitudinal dependence which is again due to the impact of residual diurnal cycle.

If zonal averages are to be used to estimate inter-satellite biases, then it is disadvantageous to separate ascending and descending passes since combining them will average out at least the 24 hour component of the diurnal cycle.

Shi and Bates [2011], as shown in their Figure 3, estimated the scene-radiance dependence of the biases using biases estimated from the zonal average method. But that will present a problem if biases are time varying. *Lindfors et al.* [2011] also considers time-invariant biases. If the biases are time varying, diurnal differences can be mis-interpreted as radiance dependence.

3.3. SNOs

The left panels of Figure 6 show biases estimated using the SNO method. As discussed in Section 1, SNOs normally occur only over narrow latitude bands near the poles (from -70 to -80 and from 70 to 80 degree latitudes), except when the equator crossing times of the two satellites become similar. This has happened for N16–N15 pair around August, 2008 and we had global SNOs [*John et al.*, 2012b]. We have also shown biases estimated from zonal average brightness temperatures of those latitude bands on the right panels for easy comparison.

The two sounding channels, Channels 1 and 2, show small inter-satellite biases throughout the life of the satellites. One of the main differences of the SNO method compared to the natural target methods for these channels is that we do not see impacts of diurnal cycle differences. There are differences between Southern and Northern hemisphere estimates, possibly due to dependence of biases on scene radiances [*John et al.*, 2012b]. Biases for Channel 1 estimated using Antarctic SNOs show a trend of about 1 K over the 10 years, but there is no such trend for biases estimated using Arctic SNOs. Biases estimated from zonal mean differences (in the right panels) show very large seasonal variations for reasons explained in Section 3.1.1 which confirms that zonal average methods are not very suitable for channels with surface influence, because the surface has higher seasonal and diurnal variability compared to the atmosphere aloft.

Biases estimated for Channel 3–5 are similar for both Arctic and Antarctic SNOs. The biases estimated using zonal averages show comparable results, but there is higher seasonal variability in biases using measurements from the southern latitude band. One interesting inference one may draw from these analyses is that it is possible to have time varying radiance dependent biases. For example, the difference between biases from southern and northern hemispheres shows seasonal patterns; during certain periods there are no differences between them and during others there are significant differences and August 2008 was one of those. *John et al.* [2012b] analysed global SNO data for this month to investigate scene-radiance dependent biases for N16–N15 and found significant radiance-dependendence.

In general, SNOs should provide the "true" inter-satellite biases in the absence of scene-radiance dependent biases. This is because SNOs are not affected by diurnal cycle differences and are thus resistant to the impact of orbital drifts. Also, impacts of clouds and inhomogeneous surfaces are minimal for this method due to stringent collocation criteria.

3.4. Impact of clouds

Though microwave measurements are less impacted by clouds than infrared or visible measurements, there can be considerable cloud impacts when strong convection is present for the sounding channels [e.g., *Hong et al.*, 2005] or when cloud liquid water is present for the window channels [e.g., *Sreerekha et al.*, 2008]. Clouds affect these channels differently.

For the window channels (Channels 1 and 2) cloud liquid water acts like water vapour and the emission from the clouds will be added to the surface emission and therefore the presence of these clouds increases the brightness temperatures. On the other hand, ice particles in deep convective clouds scatters the radiation away from the line of sight of the satellite sensor and thus decreases the brightness temperatures. This effect dominates for the sounding channels (3–5), particularly for Channel 5.

As discussed before, due to our stringent collocation criteria, clouds do not impact estimated biases from SNOs, because measurements from both satellites will be affected in somewhat similar ways. However, clouds can have significant impacts on the estimated biases when natural targets or zonal averages are used. To estimate the impact of clouds we have used the method developed by *Buehler et al.* [2007] which can be used to filter the clouds affecting Channel 3 measurements. As *Moradi et al.* [2010] demonstrated that the cloud filtering works well for the tropics, we have used tropical ocean averages to check the impact. The method is based on brightness temperature differences of Channels 3 and 5 and a threshold for Channel 3 brightness temperatures. We used data only until 2006 because after that significant biases exist for these channels and such biases can result in false cloud detection or missing a cloud. This method basically filters out clouds with ice particles, so we used it for the three sounding channels as these channels are all affected by ice scattering.

Figure 7 shows biases estimated using all (green curve) data and only clear (blue curve) over tropical ocean. It is encouraging to see that biases estimated using all and clear data are similar. Differences are small because when the data are averaged for a month cloud effects are similar for both satellites.

3.5. Scene-radiance dependent bias

As discussed in *John et al.* [2012b] inter-satellite biases in most cases depend on scene-radiance. Here we analyse how different the estimates are from polar-only collocations and global collocations. Figure 8 shows the difference between the scene-radiance dependence of the biases estimated from the two sets of collocations. We have collated biases into 10 K brightness temperature bins and then computed their mean and standard error for all bins with 100 or more data values, as done in *John et al.* [2012b]. The surface channels (1–2) show no difference because they do not have strong radiance dependence for this satellite pair [see Figure 9 of *John et al.*, 2012b]. The differences tend to get larger for the sounding channels (3–5) at warmer measurements which are not well represented in the polar subset. Therefore, the scene-radiance dependence of the biases estimated from polar-only SNOs should be used with caution.

4. Summary and outlook

In this study we have assessed three methods for inter-calibrating operational satellite microwave humidity sounders which is a necessary step towards creating climate data records from these measurements. The methods we have analysed are using : 1) simultaneous nadir overpasses (SNOs) [e.g., *Cao et al.*, 2004], 2) Antarctica and Tropical Oceans as natural targets [e.g., *Mo*, 2011], and 3) zonal averaged brightness temperatures [*Shi and Bates*, 2011]. In all methods, biases are calculated by averaging the data for a month.

One of the natural targets, Antarctica, is found to be not very suitable for calibrating microwave humidity sounding channels. Owing to its elevated surface and drier atmosphere, all channels are sensitive to the surface over Antarctica. Therefore strong diurnal and seasonal cycle and diurnal cycle aliasing (due to orbit drift of the satellites) signals are present in the estimated biases, which compromise their use for inter-calibration. Nonetheless, the results reveal some of the instrument problems and general bias patterns.

On the other hand, biases estimated using tropical ocean measurements show clear signals of bias patterns and instrument problems, because diurnal and seasonal variations of these measurements are smaller over tropical ocean. Combining ascending and descending measurements helps to overcome any residual diurnal cycle aliasing. Combining the two passes which are 12 hours apart removes the 24 hour component of the diurnal cycle, which is predominant for the surface sensitive channels [*Kottayil et al.*, 2012]. But even after combining the passes, smaller signals of diurnal cycle aliasing remain in the estimated biases for surface channels due to asymmetries in the diurnal cycle.

Both liquid and ice clouds could impact these measurements [e.g., *Sreerekha et al.*, 2008]. We have not filtered for clouds in the analyses presented here. In order to test the impact of clouds on the estimated biases, we used a cloud filtering method by *Buehler et al.* [2007] for the three sounding channels (Channels 3–5) for the tropical ocean measurements. We found similar results for both all and cloud-cleared data.

Ideally, SNOs alone could provide correct estimates of inter-satellite biases because this method is not affected by clouds (because of the stringent spatio-temporal collocation criteria) or by diurnal cycle differences (and thus the effect of orbital drift). However, because SNOs usually occur only at very high latitudes, measurements there only represent the colder end of the radiance dynamic range and therefore if the biases have scene-radiance dependence [e.g., *Shi et al.*, 2008; *Zou and Wang*, 2011; *John et al.*, 2012b], bias estimates from SNOs represent only the biases for colder brightness temperatures.

Figure 9 shows a comparison of biases estimated from SNOs and tropical ocean measurements for Channels 1 and 3. These two channels are selected owing to their very different behavior. Channel 1 is a surface channel under all-weather conditions, thus will have strong influence from the diurnal cycle and thus orbit drift of the satellites. Channel 3 has the least influence from these because of its sensitivity to the upper troposphere. The green curves are the same as those in Figure 3 and the black and the blue curves are as in Figure 6. As expected, impacts of orbital drift are clearly seen for Channel 1, and the bias estimates differ among them. The difference between estimates of southern and northern hemispheric SNOs could possibly indicate scene-radiance dependent biases in Channel 1. During boreal winter months and also during the period when equator crossing times are about the same, the bias estimates from both hemispheres are similar. All three bias estimates and patterns for Channel 3 are very similar. Bias estimates of southern hemispheric SNOs and tropical ocean are sometimes half a Kelvin apart, which depicts possible scene-radiance dependence of these biases. This is approximately 4% relative error in UTH estimates. Both methods are capable of detecting biases arising from instrument temperature variations associated with changes in sun angle changes as shown in *Zou and Wang* [2011].

The main limitaion of using zonal averaged brightness temperatures (to a lesser extent for tropical-ocean averages) for inter-calibration is the impact of diurnal cycle which aliases into the estimated biases. One way to overcome this is to use data from only those areas where diurnal cycle of the measurements is very small. It is evident from *Kottayil et al.* [2012] that these areas are channel and time dependent. Combing the methods presented in this paper and that of *Kottayil et al.* [2012] remains topic for future work.

Overall, the biases are complex and have time-, state-, and instrument-dependencies (e.g., instrument viewing angle dependent biases, as shown in *John et al.* [2012a]). Correcting the biases of these instruments, primarily designed to provide data for weather forecasting, to create climate monitoring data sets, is challenging. See *Thorne et al.* [2011] for a detailed discussion of these issues for temperature sounding channels. When using these data for climate applications, it is necessary to have a clear understanding of the detailed specification of the required measurement uncertainties and instrument deficiencies.

Acknowledgments. We thank David Parker and Roger Saunders for valuable comments. VOJ was supported by the U.K. Joint DECC and DEFRA Integrated Climate Programme - GA01101, the UK JWCRP, and EUMETSAT CMSAF. The contributions by SAB and AK were partially funded by the Swedish Science Council and the Swedish Space Board. This work contributes to COST Action ES604–Water Vapor in the Climate System (WaVaCS) and to the EUMETSAT CMSAF activities. Thanks to Lisa Neclos, NOAA CLASS for AMSU-B and MHS Level-1b data and EUMETSAT NWP-SAF for the AAPP software to process the data.

References

Allan, R. P., A. Slingo, S. F. Milton, and M. E. Brooks (2007), Evaluation of the Met Office global forecast model using Geostationary Earth Radiation Budget (GERB) data, *Q. J. R. Meteorol. Soc.*, *133*, 19932010, doi:10.1002/qj.166.

Andersson, E., E. Holm, P. Bauer, A. Beljaars, G. A. Kelly, A. P. McNally, A. J. Simmoons, J.-N. Thpaut, and A. M. Tompkins (2007), Analysis and forecast impact of the main humidity observing systems, *Q. J. R. Meteorol. Soc.*, *133*, 1473–1485, doi: 10.1002/qj.112.

Atkinson, N. C. (2001), Calibration, monitoring and validation of AMSU-B, *Adv. Space. Res.*, *28*(1), 117–126.

Bernie, D. J., E. Guilyardi, G. Madec, J. M. Slingo, and S. J. Woolnough (2007), Impact of resolving the diurnal cycle in an oceanatmosphere GCM. Part 1: a diurnally forced OGCM, *Climate Dynamics*, *29*(6), 575–590, doi:10.1007/s00382-007-0249-6.

Bonsignori, R. (2007), The Microwave Humidity Sounder (MHS): in-orbit performance assessment", in *Proc. SPIE*, *67440A*, vol. 6744, doi:10.1117/12.737986.

Buehler, S. A., M. Kuvatov, and V. O. John (2005), Scan asymmetries in AMSU-B data, *Geophys. Res. Lett.*, *32*, L24810, doi:10.1029/2005GL024747.

Buehler, S. A., M. Kuvatov, T. R. Sreerekha, V. O. John, B. Rydberg, P. Eriksson, and J. Notholt (2007), A cloud filtering method for microwave upper tropospheric humidity measurements, *Atmos. Chem. Phys.*, *7*(21), 5531–5542, doi:10.5194/acp-7-5531-2007.

Cao, C., M. Weinreb, and H. Xu (2004), Predicting simultaneous nadir overpasses among polar-orbiting meterological satellites for the intersatellite calibration of radiometers, *J. Atmos. Oceanic Technol.*, *21*, 537–542.

Cao, C., H. Xu, J. Sullivan, L. McMillin, P. Ciren, and Y. Hou (2005), Intersatellite radiance biases for the High Resolution Infrared Radiation Sounders (HIRS) onboard NOAA-15, -16, and -17 from simultaneous nadir observations, *J. Atmos. Oceanic Technol.*, *22*(4), 381–395.

Chung, E. S., B. J. Sohn, J. Schmetz, and M. Koenig (2007), Diurnal variation of upper tropospheric humidity and its relations to convective activities over tropical Africa, *Atmos. Chem. Phys.*, *7*(10), 2489–2502, doi:10.5194/acp-7-2489-2007.

Held, I. M., and B. J. Soden (2000), Water vapor feedback and global warming, *Annu. Rev. Energy Environ.*, *25*, 441–475.

Hewison, T. J., and R. W. Saunders (1996), Measurements of the amsu-b antenna pattern, *IEEE T. Geosci. Remote*, *34*(2), 405–412, doi:10.1109/36.485118.

Hong, G., G. Heygster, J. Miao, and K. Kunzi (2005), Detection of tropical deep convective clouds from AMSU-B water vapor channels measurements, *J. Geophys. Res.*, *110*(D9), D05205, doi:10.1029/2004JD004949.

Hudson, S. R., and R. E. Brandt (2005), A look at the surface-based temperature inversion on the Antarctic Plateau, *J. Climate*, *18*, 1673–1696.

Iacovazzi, R. A., and C. Cao (2008), Reducing uncertainties of SNO-estimated inter-satellite AMSU-A brightness temperature biases for surface-sensitive channels, *J. Atmos. Oceanic Technol.*, *25*, 1048–1054.

John, V. O., and S. A. Buehler (2005), Comparison of microwave satellite humidity data and radiosonde profiles: A survey of European stations, *Atmos. Chem. Phys.*, *5*, 1843–1853, doi:10.5194/acp-5-1843-2005, sRef-ID:1680-7324/acp/2005-5-1843.

John, V. O., and B. J. Soden (2007), Temperature and humidity biases in global climate models and their impact on climate feedbacks, *Geophys. Res. Lett.*, *34*, L18704, doi:10.1029/2007GL030429.

John, V. O., G. Holl, R. P. Allan, S. A. Buehler, D. E. Parker, and B. J. Soden (2011), Clear-sky biases in satellite infra-red estimates of upper tropospheric humidity and its trends, *J. Geophys. Res.*, *116*, D14108, doi:10.1029/2010JD015355.

John, V. O., G. Holl, N. C. Atkinson, and S. A. Buehler (2012a), Monitoring scan asymmetry of microwave humidity sounding channels using simultaneous all angle collocations (SAACs), *J. Geophys. Res.*, submitted, preprint available at `http://www.sat.ltu.se/members/viju/publication/inter-calib/scan_asymmet%ry.pdf`.

John, V. O., G. Holl, S. A. Buehler, B. Candy, R. W. Saunders, and D. E. Parker (2012b), Understanding inter-satellite biases of microwave humidity sounders using global simultaneous nadir overpasses, *J. Geophys. Res.*, *117*(D2), D02305, doi:10.1029/2011JD016349.

Kennedy, J. J., P. Brohan, and S. F. B. Tett (2007), A global climatology of the diurnal variations in sea-surface temperature and implications for MSU temperature trends, *Geophys. Res. Lett.*, *34*, L05712, doi:10.1029/2006GL028920.

Kleespies, T. J., and P. Watts (2007), Comparison of simulated radiances, jacobians and linear error analysis for the Microwave Humidity Sounder and the Advanced Microwave Sounding Unit-B, *Q. J. R. Meteorol. Soc.*, *132*, 3001–3010.

Kottayil, A., V. O. John, and S. A. Buehler (2012), Correcting diurnal cycle aliasing in satellite microwave humidity sounder measurements, *J. Geophys. Res.*, submitted, preprint available at `http://www.sat.ltu.se/members/ajil/publications/diurnal_cycle.pdf`.

Lindfors, A. V., I. A. Mackenzie, S. F. B. Tett, and L. Shi (2011), Climatological diurnal cycles in clear-sky brightness temperatures from the High-Resolution Infrared Radiation Sounder, *J. Atmos. Oceanic Technol.*, *28*, 1199–1205, doi:10.1175/JTECH-D-11-00093.1.

Manabe, S., and R. T. Wetherald (1967), Thermal equilibrium of the atmosphere with a given distribution of relative humidity, *J. Atmos. Sci.*, *24*(3), 241–259.

Mo, T. (2010), A Study of the NOAA Near-Nadir AMSU-A Brightness Temperatures over Antarctica, *J. Atmos. Oceanic Technol.*, *27*, 995–1004, doi:10.1175/2010JTECHA1417.1.

Mo, T. (2011), Calibration of the NOAA AMSU-A radiometers with natural test sites, *IEEE T. Geosci. Remote*, *49*(9), 3334–3342, doi:10.1109/TGRS.2011.2104417.

Mo, T., and Q. Liu (2008), A study of AMSU-A measurement of brightness temperatures over the ocean, *J. Geophys. Res.*, *113*, D17120, doi:10.1029/2008JD009784.

Moradi, I., S. A. Buehler, V. O. John, and S. Eliasson (2010), Comparing upper tropospheric humidity data from microwave satellite instruments and tropical radiosondes, *J. Geophys. Res.*, *115*, D24310, doi:10.1029/2010JD013962.

Saunders, R. W., T. J. Hewison, S. J. Stringer, and N. C. Atkinson (1995), The radiometric characterization of AMSU-B, *IEEE T. Microw. Theory*, *43*(4), 760–771.

Saunders, R. W., B. Candy, P. N. Francis, T. Blackmore, and T. Hewison (2012), Monitoring satellite radiometer biases using NWP fields, *IEEE T. Geosci. Remote*, submitted.

Shi, L., and J. J. Bates (2011), Three decades of intersatellite-calibrated High-Resolution Infrared Radiation Sounder upper tropospheric water vapor, *J. Geophys. Res.*, *116*, D04108, doi:10.1029/2010JD014847.

Shi, L., J. J. Bates, and C. Y. Cao (2008), Scene radiance-dependent intersatellite biases of hirs longwave channels, *J. Atmos. Oceanic Technol.*, *25*(12), 2219–2229, doi:10.1175/2008JTECHA1058.1.

Soden, B. J., and J. R. Lanzante (1996), An assessment of satellite and radiosonde climatologies of upper-tropospheric water vapor, *J. Climate*, *9*, 1235–1250.

Soden, B. J., D. J. Jackson, V. Ramaswamy, M. D. Schwarzkopf, and X. Huang (2005), The radiative signature of upper tropospheric moistening, *Science*, *310*(5749), 841–844, doi:10.1126/science.1115602.

Sreerekha, T. R., S. A. Buehler, U. O'Keeffe, A. Doherty, C. Emde, and V. O. John (2008), A strong ice cloud event as seen by a microwave satellite sensor: Simulations and observations, *J. Quant. Spectrosc. Radiat. Transfer*, *109*(9), 1705–1718, doi:10.1016/j.jqsrt.2007.12.023.

Thorne, P. W., J. R. Lanzante, T. C. Peterson, D. J. Seidel, and K. P. Shine (2011), Tropospheric temperature trends: history of an ongoing controversy, *Wiley Interdisciplinary Reviews: Climate Change*, *2*, 66–88, doi:10.1002/wcc.80.

Wilheit, T. T., and A. al Khalaf (1994), A simplified interpretation of the radiances from the SSM/T-2, *Met. Atm. Phys.*, *54*, 203–212.

Wood, R., C. S. Bretherton, and D. L. Hartmann (2002), Diurnal cycle of liquid water path over the subtropical and tropical oceans, *Geophys. Res. Lett.*, *29*(23), 2092, doi:10.1029/2002GL015371.

Zou, C.-Z., and W. Wang (2011), Intersatellite calibration of AMSU-A observations for weather and climate applications, *J. Geophys. Res.*, *116*, D23113, doi:10.1029/2011JD016205.

Zou, C.-Z., M. Gao, and M. D. Goldberg (2009), Error structure and atmospheric temperature trends in observations from the Microwave Sounding Unit, *J. Climate*, *22*, 1661–1681, doi:10.1175/2008JCLI2233.1.

Table 1. Channel characteristics of AMSU-B and MHS. MHS values are given in brackets, if different from AMSU-B. f_C is the central frequency of the channel, Δf is the pass band width, NEΔT is the noise equivalent temperature taken from *Kleespies and Watts* [2007]. NEΔT values are on-orbit measurements for N16 AMSU-B and N18 MHS.

Ch.	f_C [GHz]	Δf [GHz]	Pass bands	NEΔT [K]	Beam Width [deg]	Sensitive to
1	89.0	0.5	2	0.40 (0.32)	1.1 (1.11)	Surface
2	150.0 (157.0)	1.0	2	0.80 (0.53)	1.1 (1.11)	Surface
3	183.3±1.0	0.5	2	0.80 (0.50)	1.1 (1.11)	Upper Trop.
4	183.3±3.0	1.0	2	0.75 (0.41)	1.1 (1.11)	Mid Trop.
5	183.3±7.0 (183.3+7.0)	2.0	2 (1)	0.80 (0.55)	1.1 (1.11)	Lower Trop.

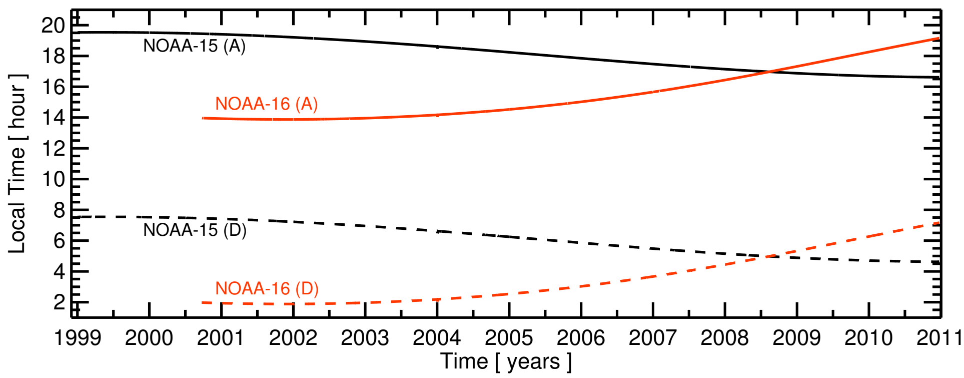

Figure 1. Local equator crossing times (LECT) of the ascending (solid lines) and descending (dashed lines) nodes of NOAA-15 and NOAA-16.

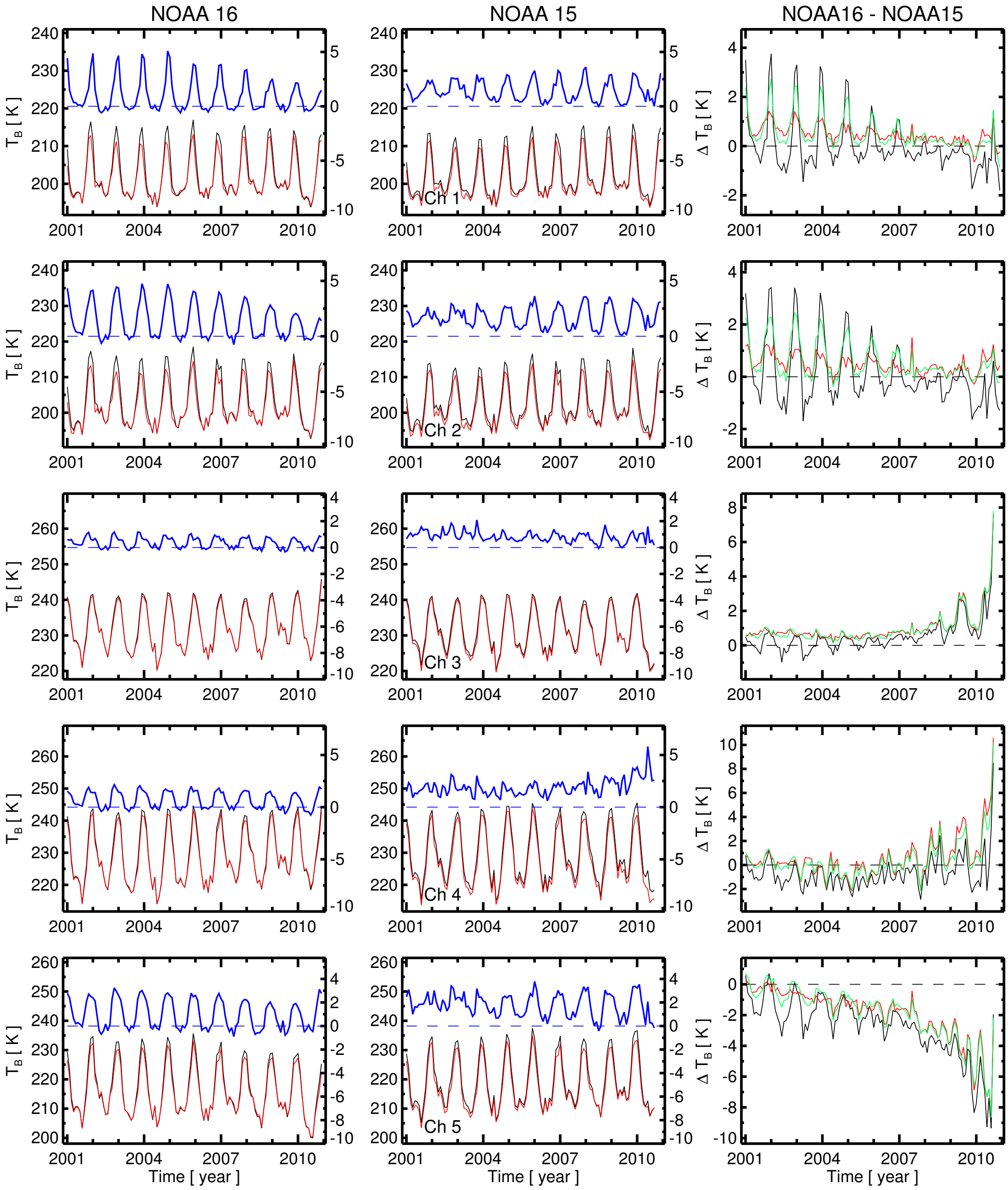

Figure 2. Monthly mean near-nadir brightness temperature for ascending (black) and descending (red) passes and their differences (blue; ascending minus descending) of NOAA-15 (middle panels) and NOAA-16 (left panels) from 2001 to 2010 over Antactica (70°S–82°S). Right panels show inter-satellite differences (N16–N15) for ascending passes (black), descending passes(red) and both combined (green).

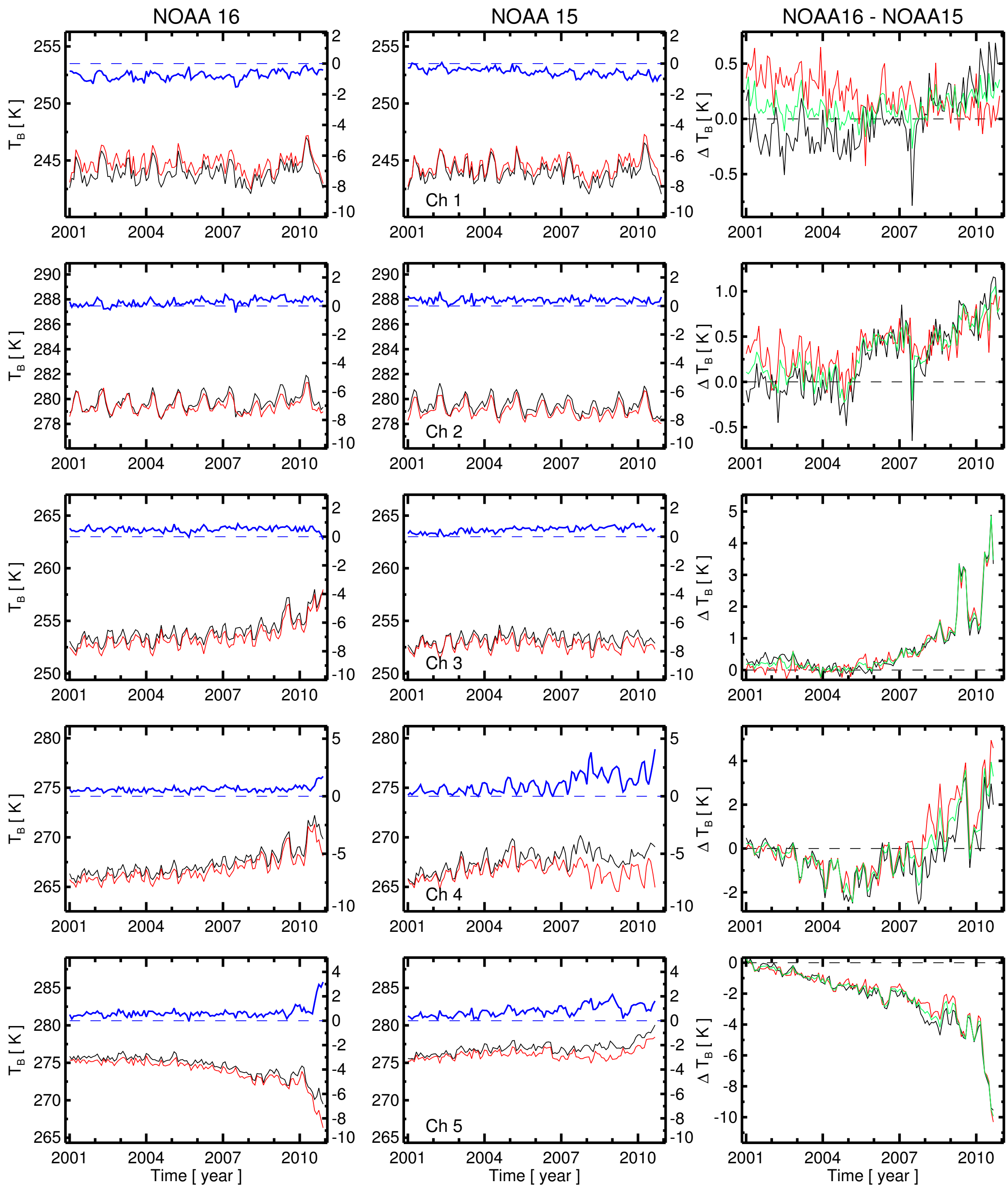

Figure 3. Monthly mean near-nadir brightness temperature for ascending (black) and descending (red) passes and their differences (blue; ascending minus descending) of NOAA-15 (middle panels) and NOAA-16 (left panels) from 2001 to 2010 over tropical oceans (20°S–20°N). Right panels show inter-satellite differences (N16–N15) for ascending passes (black), descending passes(red) and both combined (green).

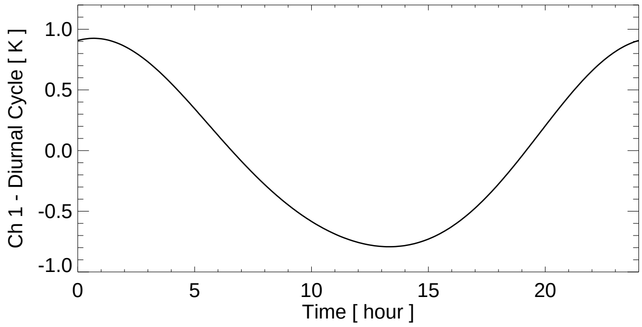

Figure 4. Diurnal cycle of Channel 1 brightness temperatures over tropical ocean. The method used to construct the diurnal cycle is described in *Kottayil et al.* [2012].

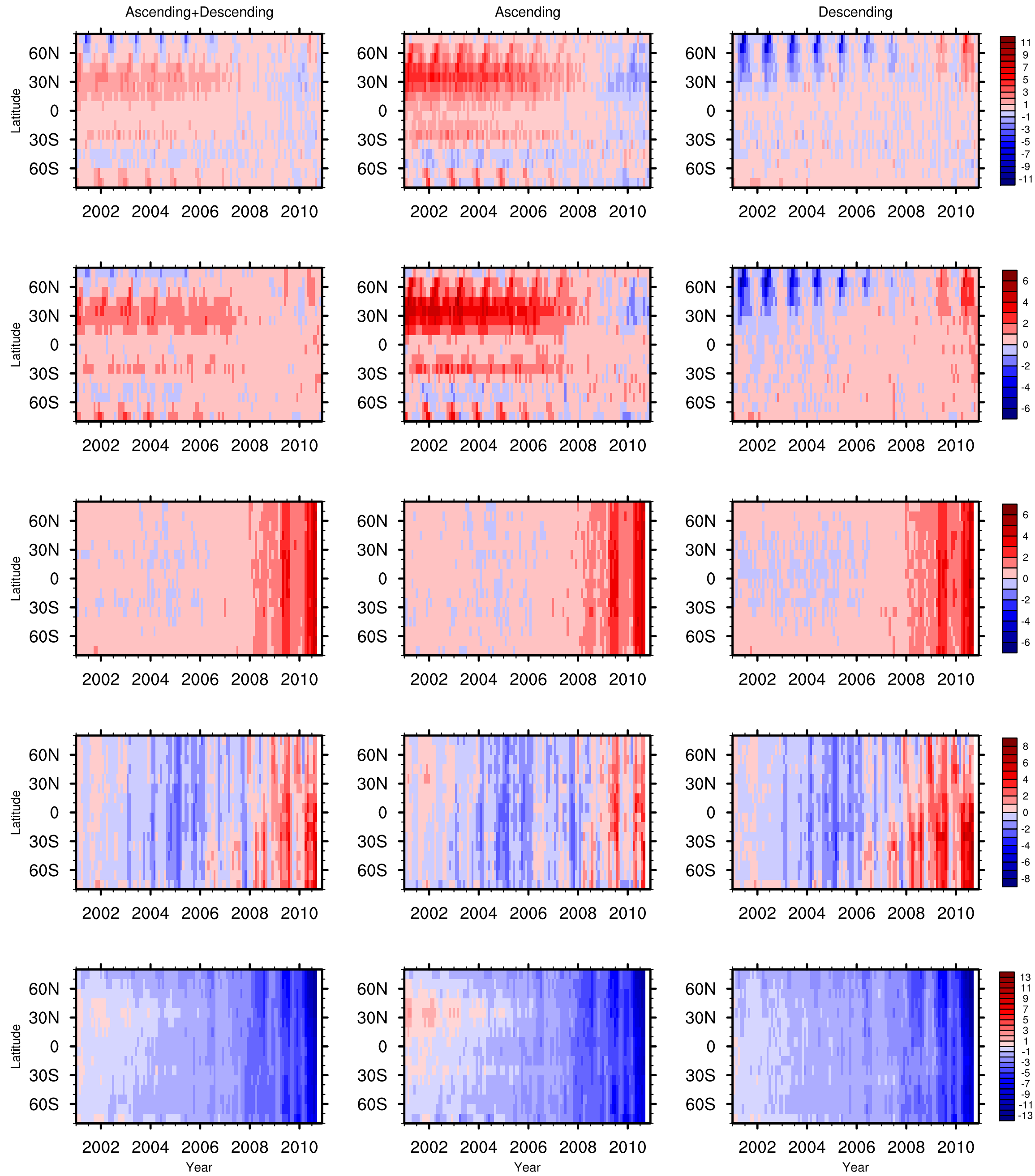

Figure 5. Biases (N16–N15, in Kelvin) estimated from zonally averaged brightness temperatures for 16 latitude bands from 80°S to 80°N in 10° intervals are shown. Channel 1 is at 1st row, Channel 2 is at the second row, and so on. Left columns show biases estimated with data which consist of both ascending and descending passes. Middle columns are biases estimated with only ascending passes and the right columns are biases estimated with only descending passes.

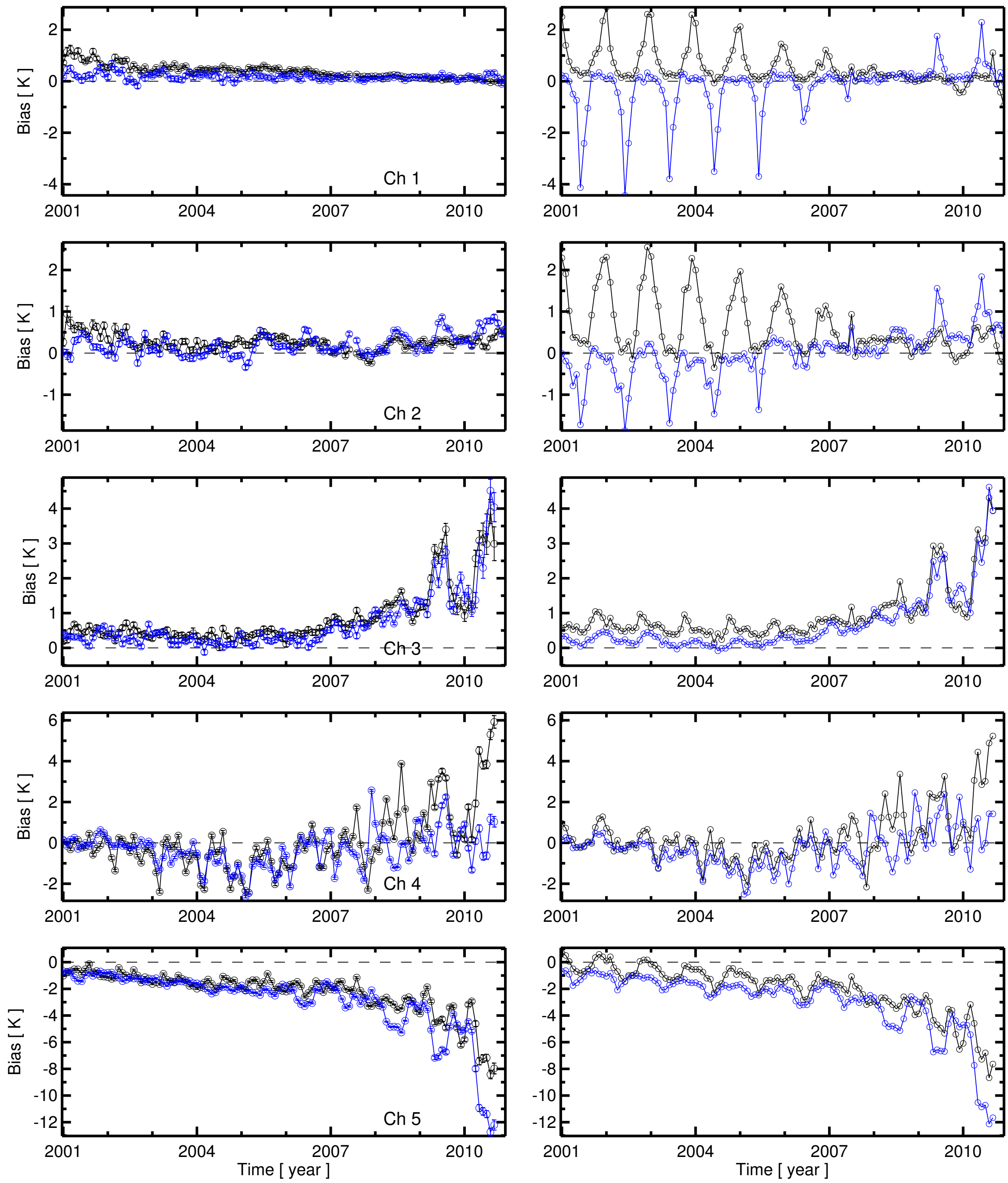

Figure 6. Left panels show inter-satellite biases (N16–N15) estimated using SNO method. Black symbols represent biases estimated using SNOs over the Antarctic and blue symbols represents biases estimated using SNOs over the Arctic. The vertical lines show standard errors of the estimated bias. Right panels show biases estimated using zonal averages (ascending and descending passes combined) for comparison where black symbols represent 70°S–80°S and blue symbols represent 70°N–80°N latitude bands. SNOs normally occur at these latitudes.

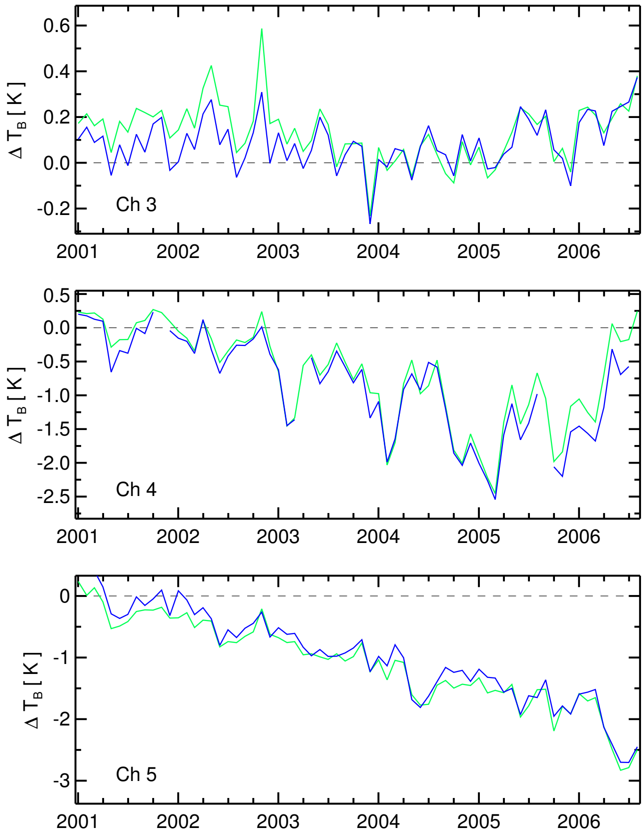

Figure 7. Impact of clouds on the estimated bias. These are tropical ocean estimates. The green curve represents all data and the blue curve represent only clear-data. Cloud filtering is based on *Buehler et al.* [2007].

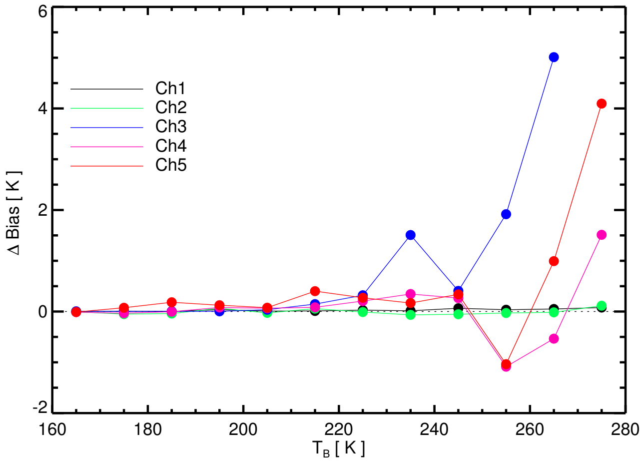

Figure 8. Difference between radiance dependence of bias computed from global collocations and only polar collocations. We used global collocations [*John et al.*, 2012b] of N15 and N16 during August 2008.

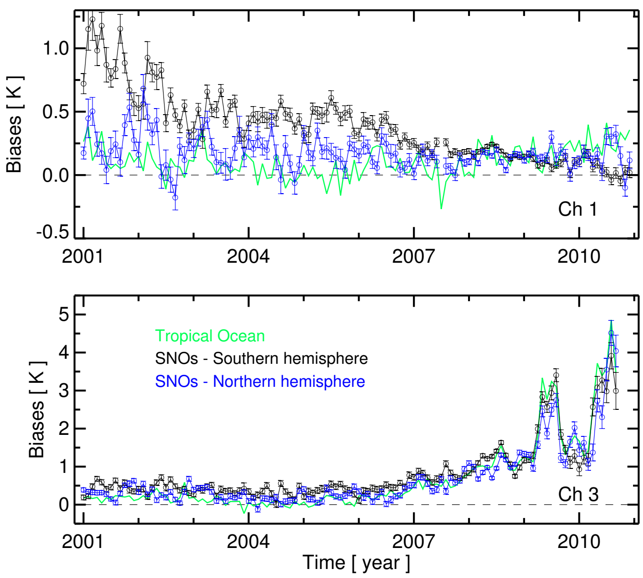

Figure 9. Bias estimates for Channels 1 and 3 using SNOs and tropical ocean measurements. SNO results from the two hemispheres are shown separately. Vertical bars for SNO bias estimates represent their standard error.